Clays and Clay Minerals, Vol. 40, No. 4, 405–420, 1992.

CHARACTERIZATION OF HYDROTHERMAL TOBELITIC VEINS FROM BLACK SHALE, OQUIRRH MOUNTAINS, UTAH

PAULA N. WILSON, W. T. PARRY, AND W. P. NASH

Department of Geology and Geophysics, 717 William Browning Building
University of Utah, Salt Lake City, Utah 84112

Abstract—Hydrothermal tobelitic phyllosilicates modeled as ISII (R3) ordering with a minimum of 2–3% and a maximum of 6–8% interstratified smectite occur in veins and as replacement of fossils in hydrothermally altered black shale. These heavy metal-rich phyllosilicate veins formed during a Mesozoic-aged, regional-scale hydrothermal event that affected an area which encompasses the Mercur Au district (Wilson and Parry, 1990a, 1990b). Associated minerals include kaolinite, quartz, chlorite, Fe-oxides, I/S (R1, 45% smectite), and pyrite. N and O contents of NH_4 phyllosilicates determined by microprobe analysis range from 0.19 to 1.78 and 48.6 to 52.9 elemental wt. %, respectively. Infrared absorption analysis indicates N occurs as NH_4^+. Very high O analyses are probably caused by contamination with kaolinite. A representative structural formula for the tobelitic material is $[(NH_4)_{0.36}K_{0.36}Na_{0.03}]$-$(Al_{1.91}Mg_{0.13}Fe_{0.03})(Si_{3.21}Al_{0.79})O_{10}(OH_{1.88}F_{0.12})$.

Correlation plots of data from microprobe analyses indicate an atypically high correlation between interlayer charge and octahedral layer charge and no correlation between (K+Na) and N. More typical correlations between N and (K+Na) and between interlayer charge and tetrahedral layer charge are obtained if 2–8% of a beidellitic smectite are factored out of the analyses. This amount of smectite is consistent with modeling of X-ray diffraction data using the computer program NEWMOD (Reynolds, 1985).

Possible sources of NH_4 are from introduction by hydrothermal fluids or from thermal degradation of organic matter prevalent within the host rocks during low-grade metamorphism. The occurrence of NH_4 phyllosilicate veins in unoxidized shale and the limited occurrence of NH_4 phyllosilicates within the host shales suggests a hydrothermal source for the NH_4.

Key Words—Ammonium illite, Hydrothermal, Microprobe, Nitrogen analysis, Tobelite.

INTRODUCTION

Tobelite and NH_4 illite are NH_4-rich analogues of illite which contain both NH_4^+ and K^+ in solid solution within the interlayer site. Tobelite is characterized by having $NH_4 > K$, Si ≥ 3 atoms, interlayer charge less than one, and a (001) spacing near 10.25 Å (Higashi, 1982). A similar phyllosilicate, but with lower NH_4^+ content ($K > NH_4$) and a smaller (001) spacing (about 10.1 Å) has been referred to as NH_4 illite (e.g., Sterne *et al.*, 1982). Reported values of N concentrations in tobelite and NH_4 illite are 1.70 to 2.07 (Higashi, 1982) and 0.24 to 1.15 wt. % N (Yamamoto and Nakahira, 1966; Sterne *et al.*, 1982; Lindgreen *et al.*, 1991), respectively. Most described NH_4-rich phyllosilicates occur in hydrothermal environments, often accompanying mineral deposits, and are associated with alteration of black shales, rhyolites, and andesites (Sterne *et al.*, 1982; Higashi, 1982; Von Damm *et al.*, 1985). Tobelite occurs as a hydrothermal alteration product of andesite and rhyolitic tuff at pottery clay and pyrophyllite deposits in Japan (Higashi, 1982). Buddingtonite, ammonioalunite, and NH_4-bearing micas have been documented as alteration products associated with precious metals in hot spring deposits (Krohn *et al.*, 1988), and NH_4 illites occur in black shales that bracket ore horizons in a shale-hosted, Pb-Zn-Ag exhalative deposit (Sterne *et al.*, 1984). NH_4-bearing phyllosilicates have also been reported in regionally metamorphosed carbonaceous pelites associated with coal seams (Juster *et al.*, 1987) and in diagenetic environments of the Gulf Coast (<0.1 wt. % N, Cooper and Abedin, 1981) and North Sea (<0.83 wt. % N, Lindgreen *et al.*, 1991).

NH_4 phyllosilicates and feldspars are probably hosts for NH_4 measured in whole-rock analyses of samples from some Mexican silver deposits (Ridgway *et al.*, 1991), from carbonate hosted Au deposits (Kydd and Levinson, 1986), from sedimentary exhalative deposits (Williams *et al.*, 1987), from precious metal and exhalative base metal deposits (Ridgway *et al.*, 1990), and from volcanic hosted Au deposits (Bloomstein *et al.*, 1987). While many of these occurrences of NH_4 anomalies are associated with mineralized veins, no vein NH_4 minerals are reported.

In nonhydrothermal environments, NH_4 is probably fixed in clay associated with crude oil and its presence is an indicator of organic maturity and migration pathways (Williams *et al.*, 1989; Williams and Ferrell, 1991). NH_4 micas are also present in metamorphic rocks where the N is of sedimentary origin (Duit *et al.*, 1986). In the laboratory, tobelite and buddingtonite have been hydrothermally synthesized (Voncken *et al.*, 1987, 1988; Shigorova *et al.*, 1981), and NH_4 has been fixed in smectite (Lagaly, 1984; Sucha and Siranova, 1991).

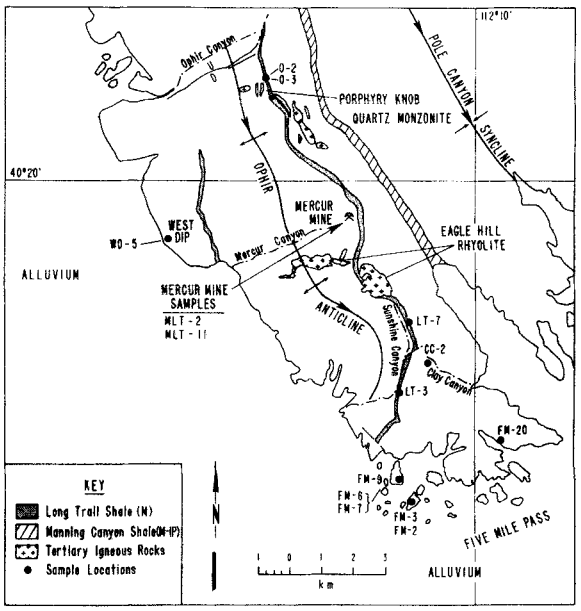

Figure 1. Generalized geologic map of the southern Oquirrh Mountains, Utah showing stratigraphic and structural relationships together with sample locations (after Gilluly, 1932).

Terminology used in this paper is that of Srodon (1984) and refers to the phyllosilicates as tobelitic material. This term indicates the presence of small amounts of interstratified smectite. I/S is used to designate R1 type interstratification and ISII indicates R3 type. In this study, we have estimated the possible range in smectite content within the illitic material using X-ray diffraction combined with simulated XRD patterns created using NEWMOD (Reynolds, 1985). The XRD modeling was then used in conjunction with modeling of chemical data obtained by microprobe analysis to place constraints on the amount of interstratified smectite. Smectite estimates from XRD have been proven valid by recent high-resolution transmission electron microscopy (HRTEM) studies in which HRTEM and X-ray diffraction techniques resulted in similar determinations of the smectite component in illitic material (Veblen *et al.*, 1990; Srodon *et al.*, 1990; Ahn and Peacor, 1989).

The purpose of this paper is to describe the occurrence, X-ray diffraction characteristics, and chemistry of hydrothermal vein tobelitic material from the southern Oquirrh Mountains of Utah. To our knowledge this is the only known vein occurrence of tobelite. Included in this discussion are microprobe analyses of the NH_4 phyllosilicates which include elemental N, O, Na, Mg, Si, Al, K, and Fe.

GENERAL GEOLOGY

The study area lies within the southern Oquirrh Mountains, 90 km southwest of Salt Lake City, Utah. Sedimentary rocks of Paleozoic age have been folded and thrust faulted, intruded by Tertiary igneous rocks, and uplifted by Basin and Range normal faulting (Gilluly, 1932). Sedimentary rocks consist of upper Paleozoic limestones, sandstones, and shales. The general geology of the study area, the spatial distribution of the strata, and sample locations are shown in Figure 1.

The NH_4 phyllosilicates occur within the Long Trail Shale which is organic-rich in its unaltered state. This unit is the middle member of the Mississippian Great Blue Limestone. The study area encompasses the Mercur Au mine, a Carlin-type deposit, where Au mineralization is hosted by the upper 60 to 80 meters of the lower limestone member of the Great Blue Limestone (Kornze, 1987). Minor Au mineralization also occurs within the Long Trail Shale which directly overlies these Au-bearing horizons (Gilluly, 1932; Wilson and Parry, 1990b). In addition to Mercur, Au has also been mined at West Dip, Sunshine Canyon, and on the ridge south of Ophir Canyon near the crest of the Ophir anticline (Figure 1). NH_4-bearing phyllosilicates occur in hydrothermally altered Long Trail Shale within the Mercur mine and throughout the surrounding region. Similarly altered shales which may be Long Trail Shale, but have never been positively correlated because they occur in structurally more complex areas and are highly altered, were sampled in the southern portion of the study area at Clay Canyon and Five Mile Pass.

SHALE HYDROTHERMAL ALTERATION

Hydrothermal alteration in the Long Trail Shale is characterized by replacement of detrital minerals by illite/smectite ranging from 2 to 40% smectite, kaolinite, Fe-oxides, chlorite, quartz, and rare dolomite. Recrystallization textures are readily apparent in thin section (Wilson and Parry, 1989). The Long Trail Shale commonly contains heavy metal-rich NH_4 phyllosilicate veins, pod-like replacements of fossils by NH_4 phyllosilicates, and is occasionally highly silicified. Altered Long Trail Shale is often oxidized, which was observed in both surface and subsurface samples, but addition of organic material during alteration appears to have occurred locally in the Mercur mine (Jewell and Parry, 1988) and at West Dip, where shales contain more organic C than any other shales: up to 3.4 wt. % (Wilson and Parry, 1990b). Oxidized and organic-rich shale enriched in As, Tl, Sb, Hg, and Sc have been found throughout the study area. Au in low ppb concentrations (6–150 ppb) has been found in the shales at West Dip, Mercur, and Sunshine Canyon (Wilson and Parry, 1990b). Oxidation results in partial to complete removal of organic material and conversion of pyrite to Fe-oxides, so that shale color varies among black, gray, white, red, or orange. In most areas oxidation is complete, but partial oxidation is observed in selvages on phyllosilicate veins with unoxidized shale left as remnant islands. The timing of oxidation is un-

certain, but K/Ar dates from veins in both oxidized and unoxidized areas are similar (Wilson and Parry, 1990a), indicating that the oxidation is either contemporaneous with the alteration, or occurred later at a temperature too low to affect K/Ar systematics. Kydd and Levinson (1986) suggest that NH_4 is completely removed from minerals in a weathering environment, but later work (Ridgway *et al.*, 1990; Krohn *et al.*, 1988) shows that NH_4 commonly occurs in surface samples.

Hydrothermal phyllosilicate veins containing tobelitic or NH_4 illitic material were found at sample localities from Ophir Canyon in the north to Five Mile Pass in the south (Figure 1). Veins usually consist of a core of discontinuous Fe-oxides replacing pyrite, or unoxidized pyrite, and borders of tobelitic or NH_4 illitic material with or without quartz. Kaolinite and rare chlorite are also found in the veins (Table 1). The phyllosilicates surround the segmented vein cores of iron oxide or sulfide minerals, indicating veins were probably single stage. The NH_4 phyllosilicates are coarse-grained (often >500 μm), white with a silky luster, and have a hair-like habit. No organic matter is apparent in the veins. The length of veins varies from a few centimeters to several meters, and the maximum vein width is 0.75 cm. Veins have a N–E trend and are subparallel to the orientation of mineralized faults in the Au deposits. The shorter veins usually occur in sets which extend discontinuously over several meters and appear to fill tension gashes. Veins are enriched in heavy metals such as Hg, As, Se, Tl, Sb, Sc, and Mo, which are commonly associated with Au mineralization. One vein (LT-3) contains 35 ppb Au (Wilson and Parry, 1990b).

The term "pod" describes a hydrothermal texture resulting from replacement of fossils by NH_4 phyllosilicates, Fe-oxides (replacing pyrite), and quartz. Pods are also found throughout the study area, occasionally with veins. They are most abundant in oxidized shale, but also occur in unoxidized shale at West Dip. The pods are elliptical and range from about 1.0 mm long by 0.1 mm wide up to 2.5 cm long by 5.0 mm wide. Pod mineralogy is identical to that of veins and usually consists of a Fe-oxide or pyritic core rimmed by coarse-grained tobelite with or without quartz, kaolinite, and chlorite (Table 1). NH_4 phyllosilicates in pods have similar physical properties to those in veins. In the pods containing both chlorite and NH_4 phyllosilicates, NH_4 phyllosilicates replace chlorite.

METHODS

Samples were collected from clay pits, road cuts, outcrops, and rarely from mine dumps at localities shown in Figure 1. Veins in the Long Trail Shale from the Mercur mine were sampled from the Sacramento and Mercur pits.

Oriented smears of vein and pod phyllosilicates were analyzed on a Phillips XRG-2600 X-ray diffractometer (CuKα) to determine the type of illitic material and degree of expandability. Samples were analyzed from 2 to 45° 2θ using a 1° slit and run speeds of 1°/min/in. Oriented smears of vein minerals were made by hand-stirring in deionized water with a 5% Calgon solution, and spreading the slurry on a glass slide. No size separations were made on vein minerals because the NH_4 phyllosilicates spontaneously disaggregate in water to micron-sized particles. Four XRD runs were made on each sample: air-dried, glycolated 24 hr at 60°C, heated 1 hr at 250°C, and heated 1 hr at 550°C. X-ray diffraction characteristics of the illitic materials found in the veins have been interpreted in terms of Ir, BB1, and BB2 parameters defined by Srodon (1984) and Srodon and Eberl (1984). Ir is the intensity ratio of the (001) to (003) diffraction peaks in an air-dried specimen divided by the intensity ratio in a glycolated specimen. The parameters BB1 and BB2 are defined as the joint breadth of the (001) and (004) illite and adjacent illite/smectite peaks, respectively. These three parameters measure the expandability and order in illite/smectite interstratifications.

Chemical analysis of the phyllosilicates was performed on a Cameca SX-50 electron microprobe with 4 multicrystal spectrometers. Analyses were made on thin section and epoxy mounted bulk material. Because there is absorption of O- and N Kα X-rays by C, the standards and unknowns were coated with C simultaneously to assure similar thicknesses of C on the surface. Our experience has shown that good analyses of O and N concentrations also require a high quality polish and flat surface. Instrumental conditions were: 15 keV accelerating voltage, 20 nA beam current, and a 10 to 20 μm diameter beam. A suite of natural minerals was used as standards for all elements except N, for which synthetic AlN was used. Both muscovite and corundum were used as standards for O. Muscovite was used in order to provide a standard similar in composition to the phyllosilicates and minimize matrix correction effects and possible changes in the shape of the OKα peak; however, there was no discernible difference in O values resulting from either standard.

The analysis of very light elements with the electron microprobe has numerous problems due, in part, to low cross-sections for ionization, high levels of absorption of the soft X-rays, and spectral interferences by higher order X-ray lines of heavier elements. Despite its abundance, O has rarely been analyzed directly, but is usually assumed by its stoichiometry with measured cations. This neglects O associated with cations not measured, notably H in hydrous silicates. The ability to determine the concentrations of O and N by electron microprobe has been greatly improved by the development of a vacuum-deposited 60 Å W/Si multilayer on a single-crystal substrate of Si (100) (Nash, 1992). This X-ray reflector is significantly superior to

Table 1. Description of samples.

Sample	Description
LT-3	Oxidized red shale consisting of illite + kaolinite + chlorite + quartz + Fe-oxides with veins and pods of NH_4 illite (R3, 2% smectite) + kaolinite + chlorite + quartz + Fe-oxides. Vertical veins strike east-west, maximum 0.25 cm wide. Fe-oxides and NH_4 illite also replace fossils.
LT-7	Gray to red-brown shale consisting of I/S (R1, 45% S) + kaolinite + quartz + minor illite. Hydrothermal veins and pods resulting from replacement of leaf fossils are abundant. Vein mineralogy is NH_4 illite + I/S (R1, 45% S) + kaolinite + minor quartz. Pod mineralogy is discrete smectite + I/S (R1, 45% S) + NH_4 illite + kaolinite + quartz.
FM-2	White, highly oxidized shale with well-developed undulating cleavage. Abundant white tobelitic veins; some up to 3 mm wide and continuous for 2 meters and oriented parallel to cleavage. Also abundant tobelitic veinlets up to 2.5 cm length and discontinuous and small pods <5 mm in diameter of same mineralogy. Veinlets are up to 40% of rock in places. Vein mineralogy is tobelite/smectite (R3, 3% S), and minor I/S (R1, 45% S), kaolinite, and quartz.
FM-3	Oxidized, highly altered, light gray, coarse-grained shale crosscut by discontinuous veins up to 0.25 cm wide of tobelite/smectite (R3, 3% S) + kaolinite + Fe-oxides + minor I/S (45% S). Shale is composed of R3 illitic material (up to 100 μm), kaolinite, and angular quartz.
FM-6	Similar to FM-2 with abundant larger tobelitic veins up to 3 mm wide and higher abundance of tobelitic veinlets (40%). Abundant fossil plant replacement. Some Fe-oxide staining. Veins consist of tobelite/smectite (R3, 3% S), very minor kaolinite, and I/S (R1, 45% S).
FM-7	Similar to FM-2, but abundance of veinlets is 20%. Vein mineralogy is tobelite/smectite (R3, 3% S), and minor kaolinite, quartz, and I/S (R1, 45% S).
FM-9	Light gray, partially oxidized shale consisting of tobelite/smectite (R3, 3% S) + kaolinite + quartz. Replacement of fossils by tobelitic material.
O-2/O-3	Light gray, oxidized, and silicified shale with veins up to 0.5 cm wide of NH_4 illite (R3, 2% S) + Fe-oxides + fibrous quartz. Fe-oxide replacement of pyrite in shale is surrounded by illite and fibrous quartz. Shale and pod mineralogy identical to veins.
CC-2	Pinkish-gray, oxidized and partially recrystallized shale. Veins up to 0.75 cm wide of NH_4 illite (R2, 2% S) + kaolinite + quartz + chlorite have attitude of N80°E, 80°S. Veins have oxidation and recrystallization selvages. Mineralogy of <4 μm size fraction of shale is R3 illitic material (7% smectite) + quartz + possible feldspar.
MLT-2	Black, organic-rich shale with white veins of NH_4 illite + chlorite + kaolinite + quartz up to 5 mm wide, 2 to 5 cm long, and discontinuous. Shale mineralogy consists of I/S (R1, 32% S) + I/S (R3, 10% S) + kaolinite + chlorite + quartz.
MLT-11	Vein of NH_4 illite (R3, 2% S) + pyrite (unoxidized) + kaolinite + chlorite + expandable unknown + gypsum in organic-rich shale. Vein 2 cm wide.
WD-5	Organic-rich shale consisting of NH_4 illite + kaolinite + quartz. NH_4 illite (R3, 2% S), chlorite, kaolinite, and minor quartz replace fossils. Small veinlets (3 cm) of same mineralogy.

crystals used previously in analysis of O and N, such as Tl acid phthalate (TAP) or Pb stearate (ODPB) (Love and Scott, 1987; Armstrong, 1988; Bastin and Heijligers, 1991a, 1991b). The synthetic reflector provides much higher peak intensities and completely suppresses higher order interfering lines, particularly partial overlaps of Al Kα (III) and Al Kα (IV) on the O and N peaks, respectively. This eliminates the need for pulse height analysis and provides a more accurate determination of the background radiation (c.f., Bastin and Heijligers, 1991b).

Concentrations were calculated from relative intensities using the $\phi(\rho z)$ method of Pouchou and Pichoir (1991) together with mass absorption coefficients from Henke *et al.* (1982) for O- and N Kα radiation. Although there is severe overlap of the Ti Ll (31.4 Å) and N Kα (31.6 Å) X-ray lines (Bastin *et al.*, 1988), in the case of the phyllosilicates in this study, Ti contents are near the limit of detection, and constructive interference with the N peak is insignificant. Peak to background ratios (P/B) for O Kα are 37 for both standard and illite containing 50% O by weight. The precision on O Kα is 0.6% of the amount present, or 0.3% O. The P/B for N Kα on the AlN standard (34.2% N) is 24; P/B on illite with 1.4% N is 2.5. Counting statistics provide a precision for N in illite containing 1.4% N of 4.8% of the amount present, equivalent to 0.08% N, which is less than the standard deviation measured for each sample (0.1–0.5 wt. %).

Infrared absorption analysis was conducted on a Biorad FTS-40 Fourier transform infrared spectroscopy unit. Five to eight milligrams of sample were mixed with approximately 150 mg of KBr. The KBr mixture was degassed for 5 min prior to application of 20,000 PSI for 5 min. Absorption spectra were obtained for the ranges of 4000 to 650 wavenumbers at a scan speed of 20 kHz and an aperture of 1 cm^{-1}.

X-RAY DIFFRACTION RESULTS

The positions of the X-ray peaks together with Ir, BB1, and BB2 values of the vein illitic minerals are shown in Table 2. Representative X-ray patterns of glycolated specimens are shown in Figure 2. Although originally determined for K-illites, we have assumed

that these parameters can also be applied to NH_4-rich illitic material. This assumption is based on the dependency of these values on the amount of smectite present in the interstratifications. Although the measurements are based on quite different absolute values of 2θ because of the differences in (001) spacing between K and NH_4 interlayer species, the values reported are changes in the peak positions caused by the presence of glycolated smectite and are relative values. Because the model on which these calculations are based assumes no interaction between illite and smectite layers (Reynolds, 1985), and the predicted type of interstratification and smectite content are the result of changes in peak positions caused by the smectite component, we have extrapolated these methods for use with NH_4 illitic material. This assumption was checked for both I/S and ISII interstratifications with NH_4 illite using the computer program NEWMOD (Reynolds, 1985) and found to be valid. For these same reasons we have also assumed that these variables can be applied to hydrothermal illitic material.

Most veins contain only one type of illitic material which is interstratified with small amounts of smectite. These phyllosilicates are only slightly expandable and comparison of glycolated and air-dry peak positions shows only small variations (Table 2). The Ir values are 1.45 to 2.45, all greater than one, and indicate the presence of at least a small amount of interstratified smectite. BB1 values of 1.9 to 3.6 and BB2 values of 1.0 to 2.8 are all less than four and indicate an ISII interstratification; however, a mixture of ISII and discrete illite is suggested by a plot of the peak positions of (002) vs. (003) (Figure 3). Most of the vein material plots within the illite field on the extreme left end of this diagram, which is consistent with the larger d-spacing of the NH_4-rich illitic layers. By Srodon's method, ISII material plotting in this field can only be said to contain <15% smectite.

Veins FM-2, FM-3, FM-6, and FM-7 have an additional illitic phase which is barely detectable on the XRD patterns. This phase is highly expandable and has BB1 values greater than four, which indicates an I/S type of interstratification with considerable smectite. Modeling of this material using NEWMOD (Reynolds, 1985) indicates it is about 45% smectite and has illite layer (001) spacings near 9.98 Å. These calculated low d-spacings indicate this material is not NH_4-bearing.

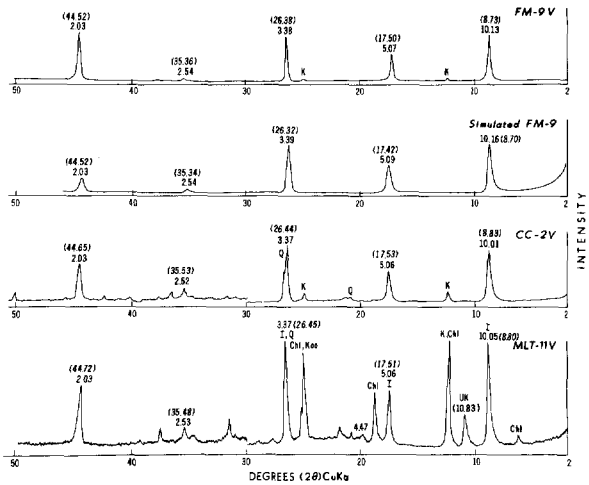

Figure 2. Representative X-ray diffraction patterns of NH_4 illitic material. A simulated pattern for sample FM-9 is shown for comparison. Peak positions in degrees 2θ are shown in parentheses. Some patterns show a change in intensity scale at 30 °2θ. Abbreviations are K = kaolinite, Q = quartz, UK = unknown, and Chl = chlorite.

The glycolated X-ray diffraction patterns in Figure 2 (FM-9V and MLT-11V) show the expanded (001) spacings of 10.13 Å and 10.05 Å typical of tobelitic materials. The pattern for CC-2 shows the separation of the quartz (101) peak from the expanded (006) peak of the tobelite. These two peaks directly overlap when the illite is K-rich.

Table 2. X-ray diffraction data for illitic vein material.

	XRD peaks (°2θ CuKα radiation)											
Sample	Glycolated					Air dried		Ir	BB1	BB2	%S	Type of illitic material
CC-2	8.83	17.53	26.44	35.53	44.65	8.73	17.51	2.34	2.0	1.3	2	ISII
FM-2	8.78	17.46	26.35	35.36	44.52	8.68	17.45	2.45	2.9	1.6	3	ISII
FM-3	8.76	17.44	26.34	35.30	44.50	8.67	17.43	2.04	2.0	2.8	3	ISII
FM-6	8.82	17.47	26.35	35.37	44.52	8.73	17.51	2.21	2.6	1.8	3	ISII
FM-7	8.75	17.50	26.39	35.34	44.51	8.73	17.49	2.29	3.0	2.0	3	ISII
FM-9	8.73	17.50	26.38	35.36	44.52	8.68	17.45	2.13	2.3	1.3	3	ISII
LT-3	8.76	17.50	26.43	35.42	44.67	8.70	17.49	1.92	1.9	1.7	2	ISII
O-2	8.83	17.61	26.5?	35.62	44.96	8.73	17.53	N.D.	2.4	1.0	2	ISII
O-3	8.89	17.68	26.6?	35.70	45.02	8.82	17.71	N.D.	3.6	1.1	2	ISII
WD-5 Pod	8.83	17.52	26.41	35.46	44.65	8.73	17.50	1.70	2.1	1.5	2	ISII

N.D. = Not determinable due to peak overlap problems with quartz.
UK = Unknown mineral.

https://doi.org/10.1346/CCMN.1992.0400405 Published online by Cambridge University Press

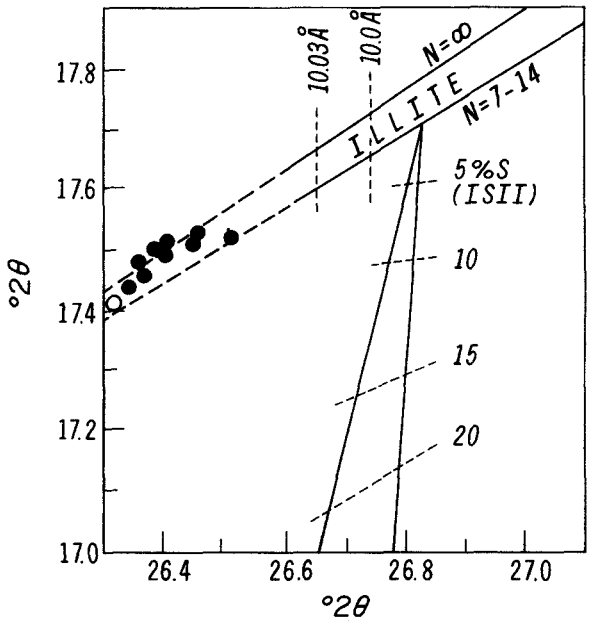

Figure 3. Plot of (002) *vs* (003) peak position for illitic materials. Samples from this study plot at extreme left of diagram, solid circles, reflecting the large (001) spacings of the NH_4-bearing illitic layers. The open circle is from the simulated pattern for sample FM-9 (after Srodon, 1984).

PHYLLOSILICATE CHEMISTRY

FTIR analysis

Representative spectra of tobelitic materials from the veins and pods are shown in Figure 4. Relative comparisons of peak heights cannot be made between samples because the data have not been normalized to account for sample weight variation in the KBr disks.

The FTIR spectrum of vein FM-9 (Figure 4A) shows the characteristics typical of illitic phyllosilicates and well-developed absorption spectra of NH_4. The spectrum of a reference sample of an NH_4-free hydrothermal sericite is shown for comparison (Figure 4B). Both spectra show strong absorption due to Si-O stretching between 1000 and 1100 cm^{-1}; Al-OH deformation near 913 cm^{-1}; O-H stretching linked to octahedral Al at 3630 and 3622 cm^{-1}; and deformation of absorbed water at about 1630 cm^{-1}. In addition, the spectrum in Figure 4B shows low and broad absorption at 3433 cm^{-1} which also results from deformation of absorbed water. Absorption lower than 970 cm^{-1} is generally caused by Al-Si-O bond deformation, although Fe-oxides also absorb in this range. The FTIR absorption spectra of the NH_4-bearing phyllosilicates show strong absorption at 1428–1439 cm^{-1} (Figures 4A, 4C, and 4D). The resonant bending frequency of NH_4^+ in mica has been reported to be 1410 cm^{-1} (Yamamoto and Nakahira, 1966), 1410–1430 cm^{-1} (Williams *et al.*, 1987), 1430 cm^{-1} (Voncken *et al.*, 1987; Vedder, 1965),

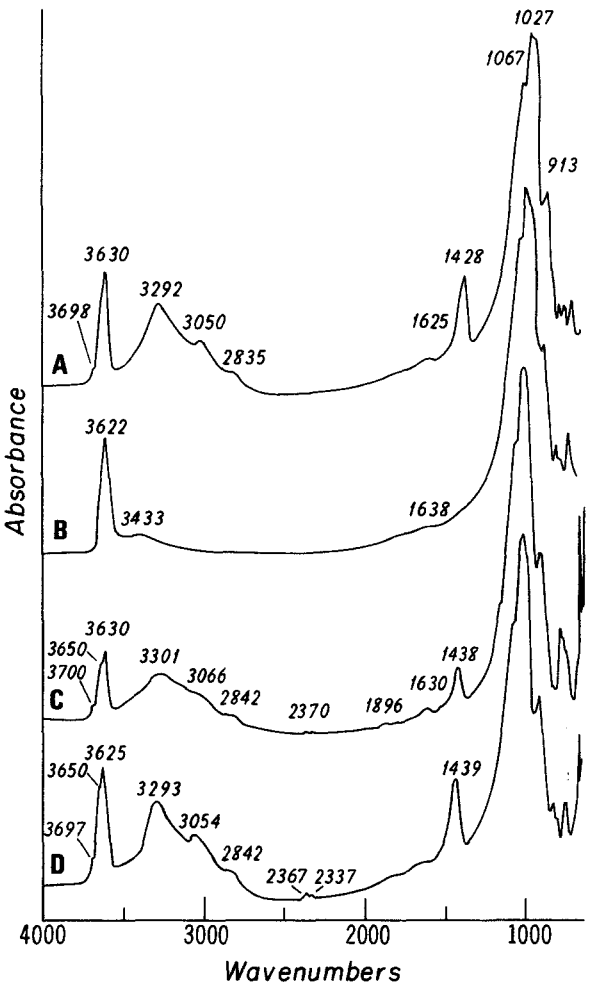

Figure 4. FTIR spectra of illitic vein and pod materials. Samples are A, FM-9 vein; B, reference muscovite from Dixie Valley, Nevada; C, CC-2 vein; and D, WD-5 pod.

1426–1428 cm^{-1} (Higashi, 1982), and 1440 cm^{-1} (Shigorova, 1982). Additional broad absorbance between 2800 and 3300 cm^{-1}, with peaks at about 3295, 3050, and 2830 cm^{-1}, represents N-H stretching as documented by Vedder (1965). The broad band between 2800 and 3300 cm^{-1} (with or without peaks) must be observed to confirm the presence of NH_4 because the strongest absorption peak for carbonates occurs near 1450 cm^{-1}. Small peaks near 3697 cm^{-1} are O-H stretching in kaolinite. NH_4 was detectable in the IR spectrum of the sample with the lowest concentration (e.g., 0.30 wt. % N) determined by microprobe analysis (Table 3).

Microprobe analysis

Representative microprobe analyses of NH_4 phyllosilicates, resulting from 101 analyses made on sam-

https://doi.org/10.1346/CCMN.1992.0400405 Published online by Cambridge University Press

ples from ten locations, are presented in Table 3. Compositional variation at each sample location is shown by one standard deviation (values in parentheses) for each element. Compositional variation between localities may be estimated by comparing average values for each element. All analyzed illitic phyllosilicates contained N but there is considerable variation, with values ranging from 0.19 to 1.88 wt. %. Other elements that vary notably are K and O. There is no obvious regional zoning of N values, but the highest N phyllosilicates come from the southern end of the range at Five Mile Pass. Sample LT-7 has the highest O content, averaging 51.4% O, probably the result of kaolinite contamination (see later section). Ca and F occur in minor amounts. The illitic phyllosilicates contain negligible amounts of Cl.

We have verified that the N concentrations indicated by the height of the 1430 cm^{-1} absorbance peak in our IR spectra are generally consistent with the N concentrations determined from microprobe methods. This was done by comparing the concentrations of N indicated by the height of the 1430 cm^{-1} absorbance peak in the IR spectra with N concentrations determined from microprobe methods. The IR spectra were normalized by calculating the ratio of absorbance due to NH_4^+ at 1430 cm^{-1} divided by the absorbance due to OH at 3630 cm^{-1}, as was done by Sterne *et al.* (1982). Then a normalized NH_4^+ absorbance versus N concentration calibration curve was determined using the spectra of analyzed NH_4-micas from Shigorova *et al.* (1981), and the measured N concentrations reported for these micas. Applying this calibration to the IR spectra in Figure 4 results in N estimates which are somewhat high relative to the microprobe data. Samples FM-9 vein, CC-2 vein, and WD-5 pod contain 1.55, 1.29, and 1.22 wt. % N, respectively, from the microprobe analyses (Table 3) and 2.02, 2.09, and 1.55 wt. % N, respectively, from the IR calibration.

In a separate technique, both XRD and IR data were used to estimate N with the methods used by Sterne *et al.* (1982). In this technique, physical mixtures of illite and NH_4Cl were analyzed by IR and the normalized NH_4^+ absorbance was plotted against the ratio of moles NH_4^+/(moles NH_4^+ + moles illite) and against 2θ (002) from XRD measurements. Comparison of normalized NH_4^+ absorbance from spectra in Figure 4 with the moles NH_4^+/(moles NH_4^+ + moles illite) calibration of Sterne *et al.* (1982) for FM-9 vein, CC-2 vein, and WD-5 pod yields mole fractions of 0.28, 0.20, and 0.25, respectively, compared with mole fractions of NH_4^+ calculated from microprobe analyses in Table 3 of 0.48, 0.39, and 0.38, respectively. Comparison of 2θ (002) of FM-9 vein, CC-2 vein, and WD-5 pod from Table 2 with the Sterne *et al.* (1982) calibration yields NH_4^+ mole fraction of 0.18 for these three samples. The IR and XRD methods of Sterne *et al.* (1982) underestimate N relative to microprobe analysis, which is consistent with their report that their methods give minimum values.

Although the NH_4^+ concentrations determined by these methods are somewhat similar to the microprobe values, a rigid comparison between the IR and microprobe methods of determining N concentrations cannot be made: the IR spectra in Figure 4 are subject to problems due to sample preparation effects, particle size effects, impure specimens, grain orientation within the pellets, and possible calcite interference in the IR spectra.

Structural formulae were calculated based on assumption of 22 negative charges. Although O data were obtained, this assumption involving O must be made unless H analyses are also acquired. Fe was assumed to have the +2 valence because of the reducing conditions indicated by the presence of NH_4^+ and pyrite, but the very low Fe values minimize any error due to the presence of possible Fe^{+3}. The average and standard deviation in the number of ions for each sample location are also presented in Table 3. The multiplying factor which resulted from assuming 22 negative charges was also applied to the O data in order to test the 12 O assumption. In most analyses, the number of moles of O varied between 11.8 and 12.2. Occasionally the moles of O were as high as 12.8, which indicates possible contamination of the analyses. Calculated structural formulae for what appeared to be illite based on microscopic and FTIR analysis of material in samples MLT-2 and MLT-11 have very low interlayer charge (Table 3). This material appears to be a mineral mixture involving illite, but attempts to model this data as such were unsuccessful.

The distinction between tobelite and NH_4 illite is shown on a plot of the atomic proportions of N vs. (K+Na) (Figure 5A). Tobelite plots on the high N side of the N = (K+Na) line shown (Higashi, 1982). Sample descriptions given in Table 1 indicate the type of NH_4 phyllosilicates, identified by both mineral chemistry and XRD properties, that were found at each sample locality. True tobelite occurs in the Five Mile Pass area based on XRD, IR, and good microprobe totals for samples FM-3 and FM-9, and lesser quality microprobe data for FM-2, FM-6, and FM-7. NH_4 illite is found at all other sample localities; however, the composition of much of the NH_4 illitic material is close to tobelite and at least one analysis at each locality is tobelite. Veins of NH_4 illite were found at locations CC-2, LT-3, MLT-2, MLT-11, 0-2/0-3. Pods and small veinlets containing NH_4 illite were also found at WD-5, FM-20, and LT-7.

The chemical data were divided into two sets based on the structural formula calculations: tobelite with "typical" structural formulae, and NH_4 phyllosilicates high in O and Al (Table 4). Both types are unusual in that they appear to have (1) a good inverse correlation between total interlayer cations and octahedral layer

https://doi.org/10.1346/CCMN.1992.0400405 Published online by Cambridge University Press

Table 3. Representative microprobe analyses of ammonium phyllosilicates presented by sample locality (values in wt. %).

No. of analyses	FM-3 vein 12	FM-9 pod 9	FM-9 vein 8	FM-20 pod 9	LT-7 pod 11
N	1.60 (0.22)[1]	1.61 (0.23)	1.55 (0.13)	1.07 (0.17)	0.82 (0.44)
O	49.9 (0.9)	50.4 (0.9)	50.6 (0.5)	50.3 (0.9)	51.4 (1.7)
Na	0.10 (0.03)	0.12 (0.05)	0.12 (0.02)	0.47 (0.20)	0.11 (0.04)
Mg	0.55 (0.03)	0.81 (0.07)	0.71 (0.07)	0.73 (0.17)	0.46 (0.21)
Si	23.3 (0.2)	23.3 (0.3)	23.0 (0.3)	22.9 (0.4)	22.9 (0.8)
Al	19.5 (0.1)	19.1 (0.3)	19.1 (0.3)	18.8 (0.4)	19.6 (0.4)
K	3.09 (0.07)	3.28 (0.22)	3.29 (0.10)	3.50 (0.53)	2.74 (1.07)
Fe	0.42 (0.04)	0.36 (0.05)	0.37 (0.03)	0.49 (0.08)	0.42 (0.16)
Ti	0.02 (0.02)	0.03 (0.02)	0.06 (0.01)	0.05 (0.02)	0.02 (0.02)
Total	98.5 (0.9)	98.9 (1.2)	98.8 (0.7)	98.3 (0.6)	98.6 (0.7)
Ca[2]	0.10 (0.02)	N.D.	0.04 (0.03)	0.02 (0.01)	N.D.
F[2]	N.D.[3]	N.D.	0.60 (0.16)	0.38 (0.10)	N.D.
Number of ions (based on 22 negative charges and Fe = Fe^{+2} and N = NH_4^+)					
NH_4	0.44 (0.06)	0.44 (0.06)	0.43 (0.04)	0.31 (0.04)	0.31 (0.13)
Na	0.02 (0)	0.02 (0.01)	0.02 (0)	0.09 (0.02)	0.02 (0)
Mg	0.09 (0)	0.13 (0.01)	0.11 (0.01)	0.13 (0.01)	0.10 (0.03)
Si	3.18 (0.02)	3.19 (0.02)	3.18 (0.03)	3.19 (0.03)	3.20 (0.03)
Al	2.76 (0.01)	2.72 (0.03)	2.74 (0.03)	2.71 (0.03)	2.77 (0.09)
K	0.30 (0.01)	0.32 (0.02)	0.33 (0.01)	0.37 (0.02)	0.31 (0.07)
Fe	0.03 (0)	0.02 (0)	0.03 (0)	0.04 (0)	0.03 (0.01)
Ti	0.00 (0)	0.00 (0)	0.00 (0)	0.00 (0)	0.00 (0)
Ca	0.00 (0)	N.D.	0.00 (0)	0.00 (0)	N.D.
F	N.D.	N.D.	0.12	0.08	N.D.
Inter. charge	0.76 (0.06)	0.78 (0.07)	0.78 (0.04)	0.76 (0.05)	0.65 (0.19)
Tet. Al	0.82 (0.02)	0.81 (0.02)	0.82 (0.03)	0.81 (0.03)	0.80 (0.03)
Oct. Al	1.94 (0.02)	1.90 (0.02)	1.92 (0.01)	1.90 (0.01)	1.97 (0.08)
Σ Oct. Cations	2.06 (0.02)	2.06 (0.02)	2.06 (0.01)	2.06 (0.02)	2.07 (0.02)
Tet. charge	−0.82 (0.02)	−0.81 (0.02)	−0.82 (0.03)	−0.81 (0.03)	−0.80 (0.03)
Oct. charge	0.06 (0.05)	0.02 (0.06)	0.03 (0.02)	0.03 (0.04)	0.15 (0.19)

[1] Data presented as averages with one standard deviation for each sample given in parentheses.
[2] Ca and F determined during separate micrprobe session and not included in matrix correction calculations.
[3] N.D. = Not Determined.

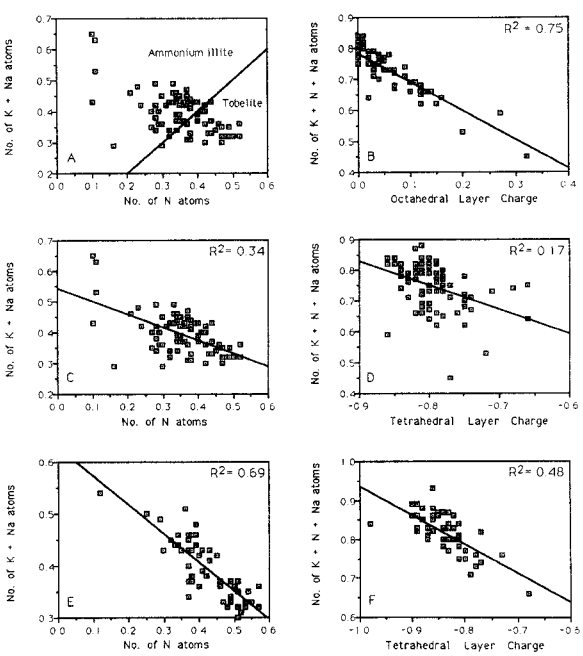

Figure 5. Correlation plots of calculated structural formula data for "typical" illitic material. Graphs A, B, C, and D are correlations from stoichiometries calculated using microprobe data. Graphs E and F are correlations from stoichiometries calculated after factoring out a beidellitic smectite. Line in graph A is where N = (K+Na). Lines in all other graphs show linear least squares fit to the data.

charge (Figures 5B and 6C), (2) no correlation between interlayer cations and tetrahedral layer charge (as shown in Figure 5D for "typical" illites), (3) octahedral cations in excess of 2.0 (Tables 3 and 4), and (4) a statistically poor correlation between atomic N and atomic (K+Na) (as shown in Figure 5C for "typical" illites), indicating no apparent substitutional relationship.

MODELING OF X-RAY DIFFRACTION DATA

The NEWMOD program (Reynolds, 1985) was used to model the X-ray diffraction data in order to estimate the amount of interstratified smectite within the NH_4 phyllosilicates. Layer charge is needed to calculate a weighted average value for the d-spacings and K content of the illitic layers. Eberl and Srodon (1988) find

https://doi.org/10.1346/CCMN.1992.0400405 Published online by Cambridge University Press

Table 3. Continued.

LT-3 vein 9	O-2/O-3 vein 12	CC-2 vein 16	WD-5 pod 2	MLT-11 vein 13	MLT-2 vein 2
1.12 (0.21)	1.03 (0.48)	1.29 (0.14)	1.22 (0.13)	0.36 (0.17)	0.30 (0.11)
50.1 (1.2)	49.3 (0.6)	50.1 (0.7)	49.9 (0.6)	50.2 (0.5)	49.6 (1.3)
0.24 (0.07)	0.16 (0.03)	0.13 (0.03)	0.10 (0.01)	0.17 (0.11)	0.22 (0.06)
0.84 (0.12)	1.03 (0.17)	0.94 (0.08)	1.08 (0.23)	0.83 (0.08)	0.39 (0.07)
23.3 (0.4)	23.5 (0.4)	23.5 (0.3)	23.3 (0.7)	23.1 (0.3)	23.1 (0.2)
18.9 (0.3)	18.2 (0.5)	18.8 (0.3)	18.6 (0.9)	19.1 (0.3)	20.1 (0.1)
3.95 (0.13)	4.54 (0.78)	3.84 (0.26)	3.05 (0.38)	4.83 (0.57)	3.09 (0.70)
0.36 (0.13)	0.44 (0.24)	0.26 (0.05)	0.40 (0)	0.04 (0.03)	0.20 (0.15)
0.05 (0.03)	0.03 (0.02)	0.04 (0.03)	N.D.	0.03 (0.02)	0.07 (0.03)
98.9 (1.3)	98.2 (0.6)	98.8 (0.7)	97.6 (0)	98.7 (0.7)	97.3 (0.2)
0.03 (0.03)	0.04 (0.03)	0.04 (0.01)	N.D.	0.03 (0.01)	0.04 (0.03)
0.16 (0.07)	0.85 (0.27)	0.62 (0.14)	N.D.	N.D.	N.D.
Number of ions (based on 22 negative charges and Fe = Fe^{+2} and N = NH_4^+)					
0.35 (0.05)	0.35 (0.09)	0.35 (0.04)	0.34 (0.03)	0.09 (0.05)	0.08 (0.03)
0.02 (0.01)	0.03 (0)	0.02 (0.01)	0.02 (0)	0.03 (0.02)	0.04 (0.01)
0.11 (0.03)	0.15 (0.02)	0.15 (0.01)	0.17 (0.04)	0.13 (0.01)	0.06 (0.01)
3.21 (0.02)	3.22 (0.04)	3.22 (0.02)	3.22 (0.07)	3.21 (0.01)	3.19 (0)
2.73 (0.05)	2.64 (0.04)	2.68 (0.03)	2.69 (0.15)	2.76 (0.02)	2.88 (0.03)
0.34 (0.04)	0.42 (0.03)	0.38 (0.03)	0.30 (0.04)	0.48 (0.06)	0.31 (0.07)
0.03 (0.01)	0.04 (0.01)	0.02 (0)	0.03 (0)	0.00 (0)	0.01 (0.01)
0.00 (0)	0.00 (0)	0.00 (0)	0.00 (0)	0.00 (0)	0.01 (0)
0.00 (0)	0.00 (0)	0.00 (0)	N.D.	0.00 (0)	0.00 (0)
0.03	0.17	0.12	N.D.	N.D.	N.D.
0.71 (0.05)	0.79 (0.06)	0.75 (0.05)	0.66 (0.07)	0.60 (0.06)	0.42 (0.11)
0.79 (0.02)	0.78 (0.04)	0.78 (0.02)	0.78 (0.07)	0.79 (0.01)	0.81 (0)
1.93 (0.03)	1.86 (0.01)	1.90 (0.02)	1.91 (0.07)	1.97 (0.02)	2.07 (0.03)
2.07 (0.01)	2.03 (0.02)	2.06 (0.02)	2.11 (0.04)	2.11 (0.02)	2.16 (0.04)
−0.79 (0.02)	−0.78 (0.04)	−0.78 (0.02)	−0.78 (0.07)	−0.79 (0.01)	−0.81 (0)
0.08 (0.06)	−0.03 (0.04)	0.02 (0.04)	0.12 (0.14)	0.18 (0.06)	0.36 (0.10)

illite layers in I/S have a fixed interlayer cation content of approximately 0.9 equivalents. Our initial modeling was based on an assumed interlayer charge of 0.8 for the illitic layers which was chosen based on microprobe data in Table 3 and the low smectite content indicated by the Ir, BB1, and BB2 values of the XRD data. The chemical data were used to determine percent of interlayer cations NH_4 and K, and these percentages were used to calculate a weighted average value for (1) the interlayer species, expressed in terms of K content, by expressing the NH_4 content of pure NH_4 illite as .56 K atoms (the ratio of electrons in these interlayer species) (Moore and Reynolds, 1989, p. 324), and (2) the d-spacings. The (001) spacings of 10.3 Å and 10.0 Å were used for NH_4 and K layers, respectively. The calculated weighted average values for the (001) spacings and interlayer species were used as starting points for NEWMOD simulations. Minor changes were required to most accurately simulate the actual XRD patterns. Values of K content, d-spacing, N (number of layers in crystallite), and percent illite layers used to create the simulated patterns and the resulting peak positions are presented in Table 5. We have not attempted to model peak shape parameters BB1 and BB2 exactly, nor have we attempted to model peak intensities. Variations of minimum crystallite size, maximum crystallite size, and size distribution do result in small shifts in peak position and small variations in BB1 and BB2.

Tobelite

As discussed in the XRD analysis section, the vein tobelite (FM-2, FM-3, FM-6, FM-7, and FM-9) can be interpreted in two ways: either as a mixture of ISII with discrete illite or as ISII only; both are consistent with BB1 and BB2 parameters less than 4 (Table 2). As previously discussed, a mixture of ISII (<15% smectite) and discrete illite is suggested by a plot of (002) vs. (003) °2θ (Srodon, 1984). However, the vein material can also be modeled as pure ISII with a minimum 3% smectite using NEWMOD (Reynolds, 1985). A comparison of the oriented powder diffraction data with the simulated patterns is shown in Table 5. The tobelitic material was modeled with a low equivalent K value (0.66) and large (001) spacings (10.15–10.16 Å) and these values are in good agreement with those calculated as weighted averages from microprobe and XRD data (0.64–0.67 and 10.14–10.17 Å). The mod-

https://doi.org/10.1346/CCMN.1992.0400405 Published online by Cambridge University Press

Table 4. Representative microprobe analyses and structural formulae for various types of ammonium phyllosilicates.

	Microprobe analyses (wt. %)									
	N	O	Na	Mg	Si	Al	K	Fe	Ti	Total
All data: 101 analyses										
Average	1.09	50.3	0.18	0.77	23.2	19.0	3.6	0.36	0.03	98.57
Std. Dev.	0.50	1.2	0.15	0.26	0.5	0.6	1.0	0.30	0.03	0.85
Typical ammonium phyllosilicate: 72 analyses										
Average	1.30	49.9	0.18	0.82	23.3	18.9	3.66	0.40	0.04	98.44
Std. Dev.	0.34	0.7	0.14	0.20	0.4	0.5	0.60	0.13	0.03	0.77
Hi O/hi Al: 17 analyses										
Average	0.91	52.2	0.13	0.59	22.9	19.5	2.8	0.31	0.0	99.4
Std. Dev.	0.52	1.2	0.06	0.31	0.7	0.6	1.1	0.13	0.0	1.3

eled minimum smectite content for individual veins is presented in Table 2.

Because of the fit of the peak positions in simulated patterns to the data, the agreement of simulated parameters with those calculated using microprobe data, and the greater simplicity of assuming one phase rather than two, we interpret the illitic material in these veins as ISII with a minimum 3% smectite. ISII ordering and smectite content were also determined by plotting XRD data on a diagram devised by Watanabe (1981) and modified by Inoue and Utada (1983) and Srodon and Eberl (1984, p. 533). The tobelites lack any detectable superlattice peak and plot as ISII ordering with <5% interstratified smectite.

Table 5. Comparison of powder diffraction data for ammonium phyllosilicates with simulated patterns.[1]

	Values used in NEWMOD (NM)							
Sample	% Illite	Equiv. % K	d (Illite)	Peak position (°2θ)				
CC-2				8.83	17.53	26.44	35.53	44.65
NM	0.98	0.66	10.12	8.75	17.49	26.42	35.50	44.74
FM-2				8.78	17.46	26.35	35.36	44.52
NM	0.97	0.73	10.15	8.75	17.42	26.33	35.39	44.57
FM-3				8.76	17.44	26.34	35.30	44.50
NM	0.97	0.66	10.16	8.70	17.42	26.32	35.34	44.52
FM-6				8.82	17.47	26.35	35.37	44.52
NM	0.97	0.66	10.15	8.75	17.42	26.33	35.39	44.57
FM-7				8.75	17.50	26.39	35.34	44.51
NM	0.97	0.66	10.16	8.70	17.42	26.32	35.34	44.52
FM-9				8.73	17.50	26.38	35.36	44.52
NM	0.97	0.66	10.16	8.70	17.42	26.32	35.34	44.52
LT-3				8.76	17.50	26.43	35.42	44.67
NM	0.98	0.66	10.13	8.74	17.46	26.39	35.46	44.70
MLT-2				8.77	17.51	26.51	35.40	44.81
NM	0.98	0.68	10.11	8.75	17.49	26.49	35.50	44.80
MLT-11				8.80	17.51	26.45	35.48	44.72
NM	0.98	0.66	10.12	8.75	17.49	26.42	35.48	44.74
O-2				8.83	17.61	26.5?	35.62	44.96
NM	0.98	0.73	10.07	8.75	17.58	26.53	35.66	44.97
O-3				8.89	17.68	26.6?	35.70	45.02
NM	0.98	0.73	10.05	8.82	17.61	26.58	35.72	45.08
WD-5 Pod				8.83	17.52	26.41	35.46	44.65
NM	0.98	0.65	10.13	8.74	17.46	26.39	35.46	44.71

[1] All patterns modeled assuming d(001) smectite = 16.9 Å and N = 3 to 30 with equal distribution of N between 3 and 30.

https://doi.org/10.1346/CCMN.1992.0400405 Published online by Cambridge University Press

Table 4. Continued.

	Structural formula: assuming 22 negative charges and Fe = Fe^{+2}											
	N	Na	Mg	Si	Al	K	Fe	Ti	Inter-layer charge	Tet. Al	Oct. Al	Oct. layer charge
	0.30	0.03	0.12	3.20	2.73	0.36	0.02	0.00	0.69	0.80	1.94	0.04
	0.14	0.03	0.04	0.04	0.10	0.09	0.02	0.00	0.16	0.04	0.08	0.07
	0.36	0.03	0.13	3.21	2.70	0.36	0.03	0.00	0.75	0.79	1.91	0.04
	0.09	0.02	0.03	0.04	0.06	0.06	0.01	0.00	0.07	0.04	0.03	0.07
	0.25	0.02	0.09	3.19	2.82	0.28	0.02	0.00	0.55	0.81	2.01	0.26
	0.14	0.01	0.05	0.03	0.14	0.11	0.01	0.00	0.24	0.03	0.12	0.26
	After factoring out 2–20 mol % kaolinite											
Average	0.31	0.04	0.11	3.22	2.68	0.43	0.04	0.00	0.78	0.78	1.90	0.00
Std. Dev.	0.06	0.02	0.03	0.07	0.10	0.02	0.01	0.00	0.06	0.07	0.03	0.01

NH_4 illite

The NH_4 illites (CC-2, LT-3, O-2/O-3, WD-5, FM-20, and LT-7) were modeled as pure ISII with 2% smectite in the same manner as the tobelitic material except that the NH_4 illitic material has considerable variation in N content and was modeled with varying values of K (0.65–0.73) and (001) spacing (10.05–10.13 Å). Simulated patterns for these samples also agree with the powder data from oriented smears (Table 5) and the variation in K content and d-spacing are consistent with weighted averages calculated from the microprobe data.

CHEMICAL MODELING

The correlation between interlayer charge and lack of correlation between (K+Na) and N obtained from the microprobe data of the "typical" illite analyses are not what is expected for minerals which are 100% illitic. Because of the evidence for interstratified smectite in the XRD patterns of the "typical" illites, small amounts of smectite were factored out of these analyses. In addition, a discrete kaolinite was factored out of this group of analyses because no reasonable interstratified species could be modeled to explain the structural formulae which were high in O and Al, and because kaolinite was observed in these XRD patterns. The results for each subset are presented below.

"Typical" structural formulae

The cation correlations previously described (Figures 5B–D; Table 4) would suggest that interlayer cation chemistry is controlled by octahedral layer chemistry and that NH_4^+ does not substitute for K^+. Correlation of the octahedral layer composition with interlayer charge has not been previously reported for illites, indicating this correlation is probably not a result of a mineral which is 100% illitic layers. The absence of a substitutional relationship between K^+ and NH_4^+ could be explained by either the presence of an unanalyzed interlayer element or the inclusion of some other mineral in the analyses. The good microprobe totals and lack of evidence for any other interlayer cation (i.e., Sr, Ba, Rb) sought using high resolution WDS scans both indicate that the analyses account for all of the elements present.

The observed relationships between octahedral and interlayer compositions are best explained as the result of differing amounts of interstratified smectite which have been included in the microprobe analyses. This interpretation was tested by factoring out a smectite of composition $K_{0.33}Al_2(Si_{3.67}Al_{0.33})O_{10}(OH)_2$ from the chemical data. A smectite was chosen because its presence was indicated by the XRD data and it is the only mineral appropriate for this environment which results in reasonable illitic structural formulae when factored out. A K-bearing and aluminous smectite was chosen because of the negligible amounts of Na and Ca in the chemical analyses (Table 3) and because of the apparent excess Al indicated by the high octahedral layer charge of the illitic material analyzed. Two to three percent of this smectite was factored out in accordance with the amount of smectite indicated by the modeling of the XRD data; the resulting structural formulae are presented as minimum values in Table 6. These new structural formulae show improved correlations between (K+Na) and N ($R^2 = 0.69$), between interlayer charge and tetrahedral layer charge ($R^2 = 0.48$), and result in an interlayer charge of 0.85. All are reasonable values for illites. These correlations based on XRD and chemical data modeling support the conclusion that the illitic material is of ISII ordering and not a mixture of illite and ISII.

Additional modeling of the chemical data indicate that the maximum amount of this smectite which can be factored out is 3–8% (average of 6%). If more than

https://doi.org/10.1346/CCMN.1992.0400405 Published online by Cambridge University Press

Table 6. Structural formulae of illitic material after factoring out minimum and maximum amounts of smectite.

Sample	N	Na	Mg	Si	Al	K	Fe	Ti	Inter-layer charge	Tet. Al	Oct. Al	Octahedral layer charge	Octa-hedral cations	Mol % inter-stratified smectite
FM-3 vein														
Average–Min % S	0.53	0.02	0.09	3.12	2.80	0.30	0.03	0.00	0.85	0.88	1.92	0.02	2.05	3
Average–Max % S	0.58	0.02	0.10	3.07	2.85	0.30	0.03	0.00	0.90	0.93	1.92	0.02	2.05	5
Stand. Dev.	0.03	0.01	0.01	0.02	0.02	0.01	0.00	0.00	0.03	0.02	0.01	0.02	0.01	0
FM-9 Pod														
Average	0.52	0.02	0.14	3.14	2.74	0.33	0.03	0.00	0.87	0.86	1.88	−0.02	2.05	3
Stand. Dev.	0.03	0.00	0.01	0.02	0.03	0.02	0.00	0.00	0.04	0.02	0.01	0.04	0.01	0
FM-9 Vein														
Average–Min % S	0.47	0.02	0.12	3.13	2.78	0.33	0.03	0.00	0.82	0.87	1.91	0.04	2.06	3
Average–Max % S	0.55	0.02	0.13	3.05	2.85	0.33	0.03	0.00	0.90	0.95	1.90	0.04	2.07	6
Stand. Dev.	0.02	0.00	0.01	0.02	0.02	0.01	0.00	0.00	0.01	0.02	0.01	0.02	0.01	1
FM-20 Pod														
Average–Min % S	0.33	0.10	0.13	3.16	2.73	0.37	0.04	0.00	0.80	0.84	1.89	0.02	2.06	2
Average–Max % S	0.40	0.12	0.16	3.06	2.81	0.38	0.05	0.01	0.90	0.94	1.87	0.02	2.08	6
Stand. Dev.	0.03	0.04	0.03	0.03	0.03	0.02	0.01	0.00	0.01	0.03	0.02	0.03	0.02	2
LT-3 Vein														
Average–Min % S	0.35	0.04	0.15	3.20	2.69	0.39	0.02	0.00	0.78	0.80	1.89	0.01	2.06	2
Average–Max % S	0.43	0.06	0.20	3.07	2.79	0.41	0.03	0.00	0.90	0.93	1.86	0.02	2.08	8
Stand. Dev.	0.02	0.01	0.02	0.02	0.02	0.01	0.00	0.00	0.01	0.02	0.01	0.04	0.02	2
O-2/O-3 Veins														
Average–Min % S	0.37	0.03	0.16	3.19	2.66	0.43	0.04	0.00	0.83	0.81	1.85	−0.03	2.06	2
Average–Max % S	0.44	0.04	0.18	3.13	2.71	0.42	0.05	0.00	0.90	0.87	1.84	−0.04	2.06	4
Stand. Dev.	0.03	0.00	0.02	0.03	0.03	0.02	0.01	0.00	0.01	0.03	0.01	0.04	0.02	2
CC-2 Vein														
Average–Min % S	0.38	0.02	0.16	3.19	2.69	0.38	0.02	0.00	0.79	0.81	1.88	0.01	2.07	2
Average–Max % S	0.47	0.03	0.20	3.08	2.77	0.39	0.02	0.00	0.90	0.92	1.85	0.01	2.08	7
Stand. Dev.	0.03	0.01	0.03	0.04	0.05	0.03	0.01	0.00	0.01	0.04	0.03	0.03	0.02	2

about 6% smectite is removed, the resulting illite structural formulae have an interlayer charge which exceeds 0.9, the maximum possible value for illite (Eberl and Srodon, 1988). Factoring out 3–8% smectite results in more improvement in the correlation between (K+Na) and N ($R^2 = 0.91$) and the loss of any correlation between interlayer charge and tetrahedral layer charge ($R^2 = 0.0$). The structural formulae representing the maximum amount of smectite which can be factored out are also presented in Table 6. This estimate of maximum smectite content is consistent with modeling based on NEWMOD, where simulated peak positions of ISII with 5% smectite begin to show significant deviations from the experimentally derived peaks. Assuming the chemical modeling accurately represents the structural formulae, it would appear that the estimates of the amount of interstratified smectite determined from the XRD data are within 5% or less of the actual values.

Factoring out K-spar or quartz does not result in reasonable structural formulae. Factoring out 3 mol % K-feldspar removes too much K and Si and results in illitic formulae with low interlayer charge (0.70), too much tetrahedral Al (1.0), and too much oxygen (13.7 atoms). Factoring out quartz also results in interlayer charges which are low. A maximum interlayer charge of 0.85 is obtained if the tetrahedral layer charge is allowed to increase to a value of 1.0 when 20 mol % quartz is removed. This is an unreasonably high tetrahedral layer charge for illite (Srodon and Eberl, 1984; Newman and Brown, 1987) or tobelite (Higashi, 1982) and 20 mol % of a quartz contaminant (approximately 5 wt. %) should have been detectable using the XRD because the quartz (101) peak does not directly overlie the tobelite (006) peak as it does the K-rich illite (006) peak (see CC-2V in Figure 3). Quartz was not detected by XRD in several of the veins (Table 1) and quartz was not apparent during microscopic evaluation of the analyzed sites.

High O/high Al NH_4 minerals

The high O/high Al analyses are presented in Table 4. These analyses have relatively high total weight percent O and Al, low interlayer charge, and a very high octahedral charge (Table 4). In addition to the correlations common to all analyses, this data set also has (1) a positive correlation between octahedral layer charge and atomic O ($R^2 = 0.90$; Figure 6A), (2) a negative correlation between total interlayer cations and atomic O ($R^2 = 0.87$; Figure 6B), (3) an inverse correlation between interlayer cations and octahedral layer charge ($R^2 = 1.0$; Figure 6C), (4) a positive correlation between total atomic Al and atomic O ($R^2 = 0.94$; Figure 6D), and (5) a negative correlation between interlayer charge and atomic Al ($R^2 = 0.94$; Figure 6E).

The high O content of some analyses and their inverse correlation between interlayer charge and atomic O could in part be a result of varying H_3O^+ content in the interlayer site. However, assuming a maximum interlayer site occupancy of 0.9, the allowable H_3O^+ content is insufficient to account for all of the O present. In addition, the high Al values and high octahedral layer charge are not explained by the presence of H_3O^+. A more likely explanation can be made by assuming that the data represent mineral mixtures. XRD and IR data indicate that discrete kaolinite is common in most samples and that quartz and smectite also occur (Table 1); occasionally these minerals can be identified optically.

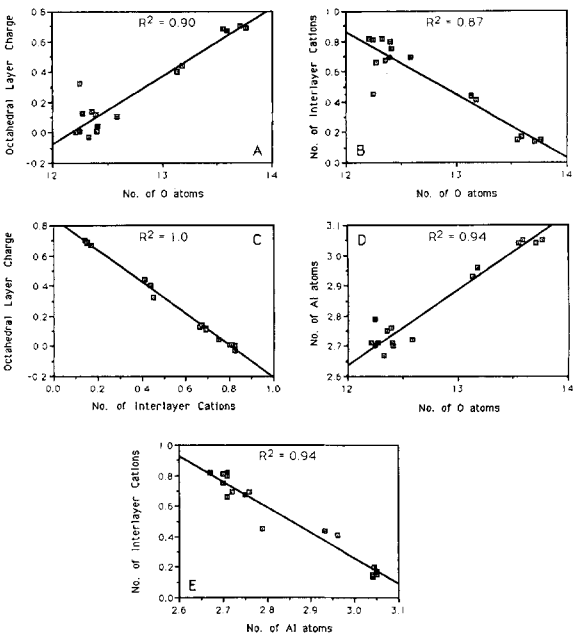

Figure 6. Correlation plots of calculated structural formulae data from the high O/high Al set of illitic microprobe analyses.

The high Al, high O, low total interlayer cations, high octahedral layer charge, and resulting correlations could be the result of contamination of the microprobe analyses by kaolinite. To test this, kaolinite was factored out of each of the chemical analyses in this group by an iterative process which was controlled by assuming an octahedral layer charge of zero, as is the case in the "typical" analyses (Table 4). After factoring out up to 20% kaolinite from the analyses, the resulting structural formulae are consistent with the "typical" analyses (Table 4). Factoring out smectite, K-spar, and quartz did not result in reasonable structural formulae.

DISCUSSION

Tobelite and NH_4 illite are present in veins in hydrothermally altered host shale from throughout the

https://doi.org/10.1346/CCMN.1992.0400405 Published online by Cambridge University Press

southern Oquirrh Mountains. There is no apparent regional zonation to the NH_4 content in the phyllosilicates except that the highest NH_4 contents occur in the southern end of the study area where structural complexity and degree of alteration in the shale unit are highest.

NH_4-bearing minerals occur predominantly in the veins and have occasionally been positively identified in whole rock shales which contain abundant NH_4 phyllosilicate veins. The Long Trail Shale contains up to 3.4 wt. % organic C in the study area, but most of this shale is oxidized and the C content is low. The NH_4 illites occur both in the oxidized and unoxidized shales and are predominantly a vein feature. This suggests hydrothermal emplacement of the NH_4 minerals rather than derivation of NH_4 from thermal degradation of organic material within the shale during low grade metamorphism. K/Ar dating of the NH_4 phyllosilicates shows vein formation is Mesozoic in age (Wilson and Parry, 1990a) and significantly later than the time of maximum stratigraphic thickness within the encompassing Oquirrh Basin (Pennsylvanian) when low grade burial metamorphism would have been most likely to occur. In addition, the heavy metal content of the veins is many times higher than the shales, suggesting a hydrothermal emplacement of these metals (Wilson and Parry, 1990b). Similar conclusions favoring an external source for NH_4 were drawn by Juster *et al.* (1987) for formation of NH_4 illites spatially associated with metamorphosed coal beds; and by Sterne *et al.* (1982) for NH_4 illites spatially associated with stratiform base metal mineralization. In both studies, the NH_4 phyllosilicates did not occur in organic-rich pelitic rocks spatially removed from the coal or the base metal mineralization, even though the organic content was as high as 15%. NH_4 phyllosilicates in Japan are not associated with organic-rich sediments and a magmatic source for NH_4 has been suggested.

NH_4 phyllosilicate veins may be genetically linked to Au mineralization within the Mercur district. The presence of the heavy metals that are abundant in the Mercur Au deposits (As, Tl, Hg, Se, and minor Au) in both the veins and the most highly altered shales and the identical alteration assemblages in the most highly altered Long Trail Shale and in argillic alteration of limestone at Mercur indicates that the same hydrothermal event could have been responsible for both NH_4 phyllosilicates and Au mineralization. Au and NH_4 illites have been shown to be related in other types of Au deposits (Krohn *et al.*, 1988; Kydd and Levinson, 1986) and further work is currently in progress to test this relationship at Mercur.

CONCLUSIONS

Tobelitic phyllosilicates modeled as having ISII (R3) ordering and a minimum of 2–3% and a maximum of 6–8% smectite occur in veins and as replacement of fossils in hydrothermally altered black shale in the southern Oquirrh Mountains of north-central Utah. This is the only reported vein occurrence of tobelite. These phyllosilicate veins are enriched in heavy metals and formed during a Mesozoic, regional hydrothermal event that affected an area which encompasses the Mercur Au district (Wilson and Parry, 1990a, 1990b). Associated minerals include kaolinite, quartz, chlorite, Fe-oxides, interstratified illite/smectite (R1, 45% smectite), and pyrite. A typical structural formulae for the tobelite is $[(NH_4)_{0.36}K_{0.36}Na_{0.03}](Al_{1.91}Mg_{0.13}Fe_{0.03})(Si_{3.21}Al_{0.79})O_{10}(OH_{1.88}F_{0.12})$. Infrared absorption analysis indicates N occurs as NH_4.

Correlation plots of data from microprobe analyses indicate an atypically high correlation between interlayer charge and octahedral layer charge and no correlation between (K+Na) and N, indicating no substitutional relationship. More typical correlations between N and (K+Na) and between interlayer charge and tetrahedral layer charge are obtained if 2–8% of a beidellitic smectite are factored out of the analyses. This amount of smectite is consistent with modeling of X-ray diffraction data using the computer program NEWMOD (Reynolds, 1985). Analyses very high in O and Al are modeled as contamination of microprobe analyses by kaolinite. Some analyses very low in interlayer cations remain unidentified.

Possible sources of NH_4 are introduction by hydrothermal fluids or from thermal degradation of organic matter prevalent within the host rocks during low-grade metamorphism. The occurrence of NH_4 phyllosilicate veins in unoxidized shale, the age of the veins, and the limited occurrence of NH_4 phyllosilicates within any of the shales suggests a hydrothermal source for the NH_4.

ACKNOWLEDGMENTS

Financial support was given by Utah Geological Survey, the University of Utah Mineral Leasing Fund, and Barrick-Mercur Gold Mines. We thank T. Shrier for access to the Mercur mine and to drill samples and logs, Prochnau Mining and Gold Standard for providing access to properties, J. Miller and K. Bukka for access to FTIR facilities, and F. Brown for reviewing an earlier version of this manuscript. The electron microprobe was purchased with financial assistance from the National Science Foundation and the University of Utah.

REFERENCES

Ahn, J. H. and Peacor, D. R. (1989) Illite/smectite from Gulf Coast shales: A reappraisal of transmission electron microscope images: *Clays & Clay Minerals* **37**, 542–546.

Armstrong, J. T. (1988) Accurate quantitative analysis of oxygen and nitrogen with a W/Si multilayer crystal: in *Microbeam Analysis-1988*, D. E. Newbury, ed., San Francisco Press, 301–304.

Bastin, C. F. and Heijligers, H. J. M. (1991a) Quantitative electron probe microanalysis of ultra-light elements (boron-oxygen): in *Electron Probe Quantitation,* K. F. J. Heinrich and D. E. Newbury, eds., Plenum Press, New York, 145–161.

Bastin, C. F. and Heijligers, H. J. M. (1991b) Quantitative electron probe microanalysis of nitrogen: *Scanning* **13,** 325–342.

Bastin, C. F., Heijligers, H. J. M., and Pinxter, J. F. (1988) Quantitative EPMA of nitrogen in Ti-N compounds: in *Microbeam Analysis-1988,* D. E. Newbury, ed., San Francisco Press, 290–294.

Bloomstein, E., Kydd, R. A., and Levinson, A. A. (1987) Development of ammonium geochemistry as a new technique in precious and base metals exploration: *Journal of Geochemical Exploration* **29,** 386.

Cooper, J. E. and Abedin, K. E. (1981) The relationship between fixed ammonium-nitrogen and potassium in clays from a deep well on the Texas Gulf Coast: *Texas Journal of Science* **33,** 103–111.

Duit, W., Jansen, J. B. H., Breemen, A. V., and Bos, A. (1986) Ammonium micas in metamorphic rocks as exemplified by Dome de L'Agout (France): *Amer. J. Sci.* **286,** 702–732.

Eberl, D. D. and Srodon, J. (1988) Ostwald ripening and interparticle-diffraction effects for illite crystals: *Amer. Mineral.* **73,** 1335–1345.

Gilluly, J. (1932) Geology and ore deposits of the Stockton and Fairfield quadrangles, Utah: U.S. Geo. Survey Prof. Paper 173, 171 p.

Henke, B. L., Lee, P., Tanake, T. J., Shimabukuro, and Fujikawa, B. K. (1982) Low-energy X-ray interaction coefficients: Photoabsorption, scattering, and reflection: *Atomic Data and Nuclear Data Tables* **27,** 1–144.

Higashi, S. (1982) Tobelite, a new ammonium dioctahedral mica: *Mineralogical Journal* **11,** 138–146.

Inoue, A. and Utada, M. (1983) Further investigations of a conversion series of dioctahedral mica/smectites in the Shinzan hydrothermal alteration area, northeast Japan: *Clays & Clay Minerals* **31,** 401–412.

Jewell, P. W. and Parry, W. T. (1988) Geochemistry of the Mercur gold deposit (Utah, U.S.A.): *Chemical Geology* **69,** 245–265.

Juster, T. C., Brown, P. E., and Bailey, S. W. (1987) NH_4-bearing illite in very low grade metamorphic rocks associated with coal, northeastern Pennsylvania: *Amer. Mineral.* **72,** 555–565.

Kornze, L. D. (1987) Geology of the Mercur gold mine: in *Bulk Mineable Precious Metal Deposits of the Western United States, Guidebook for Field Trips,* The Geological Society of Nevada, 381–389.

Krohn, M. D., Altaner, S. P., and Hayba, D. O. (1988) Distribution of ammonium minerals at Hg/Au-bearing hot spring deposits: Initial evidence from near-infrared spectral properties: in *Bulk Mineable Precious Metal Deposits of the Western United States, Symposium Proceedings,* R. W. Schafer, J. J. Cooper, and P. G. Vikre, eds., The Geological Society of Nevada, 661–679.

Kydd, R. A. and Levinson, A. A. (1986) Ammonium halos in lithogeochemical exploration for gold at the Horse Canyon carbonate-hosted deposit, Nevada, U.S.A.: Use and limitations: *Applied Geochemistry* **1,** 407–417.

Lagaly, G. (1984) Clay-organic reactions: *Phil. Trans. R. Soc. London* **A311,** 315–332.

Lindgreen, H., Jacobsen, H., and Jakobsen, H. J. (1991) Diagenetic structural transformations in North Sea Jurassic illite/smectite: *Clays & Clay Minerals* **39,** 54–69.

Love, G. and Scott, V. D. (1987) Progress in the EPMA of light elements: *Inst. Phys. Conf. Ser.* No. 90, Chapter 11, 349–352.

Moore, D. M. and Reynolds, R. C. (1989) *X-ray Diffraction and the Identification Analysis of Clay Minerals*: Oxford University Press, New York, 332 pp.

Nash, W. P. (1992) Analysis of oxygen with the electron microprobe: Applications to hydrated glass and minerals: *Amer. Mineral.* **77,** 453–456.

Newman, A. C. D. and Brown, G. (1987) The chemical constitution of clays: in *Chemistry of Clays and Clay Minerals,* A. C. D. Newman, ed., John Wiley and Sons, New York, 1–128.

Pouchou, J. L. and Pichoir, F. (1991) Quantitative analysis of homogeneous or stratified microvolumes applying the model "PAP": in *Electron Probe Quantitation,* K. F. J. Heinrich and D. E. Newbury, eds., Plenum Press, New York, 31–75.

Reynolds, R. C. (1985) *Description of Program NEWMOD for the Calculation of the One-dimensional X-ray Diffraction Patterns of Mixed-layered Clays:* Dept. of Earth Sciences, Dartmouth College, Hanover, New Hampshire, 23 pp.

Ridgway, J., Appleton, J. D., and Levinson, A. A. (1990) Ammonium geochemistry in mineral exploration—A comparison of results from the American cordilleras and the southwest Pacific: *Applied Geochemistry* **5,** 475–489.

Ridgway, J., Martiny, B., Gomez-Caballero, A., Macias-Romo, C., and Villasenor-Cabral, M. G. (1991) Ammonium geochemistry of some Mexican silver deposits: *Journal of Geochemical Exploration* **40,** 311–327.

Shigorova, T. A. (1982) The possibility of determining ammonium content of mica by IR spectroscopy: *Geochemistry International* **19 No. 2,** 110–114.

Shigorova, T. A., Kotov, N. V., Kotel'nikova, Ye. N., Shmakin, B. M., and Frank-Kamenetskiy, V. A. (1981) Synthesis, diffractometry, and IR spectroscopy of micas in the series from muscovite to the ammonium analog: *Geochemistry International* **18 No. 3,** 76–82.

Srodon, J. (1984) X-ray powder diffraction identification of illitic materials: *Clays & Clay Minerals* **32,** 337–349.

Srodon, J. and Eberl, D. D. (1984) Illite: in *Micas,* S. W. Bailey, ed., *Reviews in Mineralogy* **3,** Mineralogical Society of America, Washington, D.C., 495–544.

Srodon, J., Andreoli, C., Elsass, F., and Robert, M. (1990) Direct high-resolution transmission electron microscopic measurement of expandability of mixed-layer illite/smectite in bentonite rock: *Clays & Clay Minerals* **38,** 373–379.

Sterne, E. J., Reynolds, R. C., Jr., and Zantop, H. (1982) Natural ammonium illites from black shales hosting a stratiform base metal deposit, DeLong Mountains, Northern Alaska: *Clays & Clay Minerals* **30,** 161–166.

Sterne, E. J., Zantop, H., and Reynolds, R. C. (1984) Clay mineralogy and carbon-nitrogen geochemistry of the Lik and Competition Creek zinc-lead-silver prospects, DeLong Mountains, Alaska: *Economic Geology* **79,** 1406–1411.

Sucha, V. and Siranova, V. (1991) Ammonium and potassium fixation in smectite by wetting and drying: *Clays & Clay Minerals* **39,** 556–559.

Veblen, D. R., Guthrie, G. D., Livi, K. J. T., and Reynolds, R. C. (1990) High-resolution transmission electron microscopy and electron diffraction of mixed-layer illite/smectite: Experimental results: *Clays & Clay Minerals* **38,** 1–13.

Vedder, W. (1965) Ammonium muscovite: *Geochim. Cosmochim. Acta* **29,** 221–228.

Voncken, J. H. L., Konings, R. J. M., Jansen, J. B. H., and Woensdregt, C. F. (1988) Hydrothermally grown buddingtonite, an anyhydrous ammonium feldspar ($NH_4AlSi_3O_8$): *Physics and Chemistry of Minerals* **15,** 323–328.

Voncken, J. H. L., Wevers, J. M. A. R., van der Eerden, A. M. J., Bos, A., and Jansen, J. B. H. (1987) Hydrothermal

synthesis of tobelite, $NH_4Al_2Si_3AlO_{10}(OH)_2$ from various starting materials and implications for its occurrence in nature: *Geologie en Mijnbouw* **66,** 259–269.

Von Damm, K. L., Edmond, J. M., Measures, C. I., and Grant, B. (1985) Chemistry of submarine hydrothermal solutions at Guaymas Basin, Gulf of California: *Geochim Cosmochim. Acta* **49,** 2221–2237.

Watanabe, T. (1981) Identification of illite/montmorillonite interstratifications by X-ray powder diffraction: *J. Miner. Soc. Japan, Spec. Issue* **15,** 32–41 (in Japanese).

Williams, L. B. and Ferrell, R. E., Jr. (1991) Ammonium substitution in illite during maturation of organic matter: *Clays & Clay Minerals* **39,** 400–408.

Williams, L. B., Zantop, H., and Reynolds, R. C. (1987) Ammonium silicates associated with sedimentary exhalative ore deposits: a geochemical exploration tool: *Journal of Geochemical Exploration* **27,** 125–141.

Williams, L. B., Ferrell, R. E., Jr., Chinn, E. W., and Sassen, R. (1989) Fixed-ammonium in clays associated with crude oils: *Applied Geochemistry* **4,** 605–616.

Wilson, P. N. and Parry, W. T. (1989) Geochemical characteristics of hydrothermally altered black shales of the southern Oquirrh Mountains and relationships to Mercur-type gold deposits: *Utah Geol. and Mineral Survey Open File Report 161,* 64 pp.

Wilson, P. N. and Parry, W. T. (1990a) Mesozoic hydrothermal alteration associated with gold mineralization in the Mercur district, Utah: *Geology* **18,** 866–869.

Wilson, P. N. and Parry, W. T. (1990b) Geochemistry of Mesozoic hydrothermal alteration of black shales associated with Mercur-type gold deposits: in *Gold '90, Proceedings from the Gold '90 Symposium,* D. M. Hausen, D. N. Halbe, E. U. Petersen, and W. J. Tafuri, eds., Salt Lake City, Utah, February 26 to March 1, 1990, Society of Mining, Metallurgy and Exploration, Inc., Littleton, Colorado, 167–174.

Yamamoto, T. and Nakahira, M. (1966) Ammonium ions in sericites: *Amer. Mineral.* **51,** 1775–1778.

(Received 28 October 1991; accepted 20 July 1992; Ms. 2152)